

Radial-angular coupling in self-phase-modulation with structured lightM. Gil de Oliveira ¹, L. J. Pereira,¹ A. S. Santos,² K. Dechoum ¹, A. Bramati ³ and A. Z. Khoury ^{1,*}¹*Instituto de Física, Universidade Federal Fluminense, 24210-346 Niterói, Rio de Janeiro, Brazil*²*Centro Brasileiro de Pesquisas Físicas, 22290-180 Rio de Janeiro, Rio de Janeiro, Brazil*³*Laboratoire Kastler Brossel, Paris, France*

(Received 28 April 2023; accepted 26 June 2023; published 10 July 2023)

In this work we study the evolution of an optical vortex undergoing self-phase modulation inside a nonlinear Kerr medium. The intensity-dependent phase evolution couples the angular and radial degrees of freedom of the input vortex, giving rise to a rich dynamics where new radial modes are created. In the short propagation range, this dynamics is well described by a perturbative approach, predicting the generation of modes with radial numbers between zero and the absolute value of the vortex topological charge. This prediction is confirmed by numerical simulations of the nonlinear propagation equation.

DOI: [10.1103/PhysRevA.108.013503](https://doi.org/10.1103/PhysRevA.108.013503)**I. INTRODUCTION**

The role played by the orbital angular momentum (OAM) of light in nonlinear optical processes was investigated in seminal works on second harmonic generation [1,2] and parametric down conversion [3,4]. Recently, it has received renewed attention due to the rich dynamics involved and potential implications in quantum optical processes. As a research field on its own, OAM has become an important tool in optical communications, where multiplexing techniques are investigated [5–7]. In centrosymmetric media, such as atomic vapors and glasses, the nonlinear electric susceptibility can only display odd orders [8]. Self-phase modulation is an important effect associated with the cubic nonlinearity, causing amplitude-phase coupling along the propagation of a sufficiently intense beam. This amplitude-phase coupling affects the beam shape evolution as a result of self-focusing, a remarkable effect also present in the dynamics of Bose-Einstein condensates described by the Gross-Pitaevsky equation in the mean-field approximation [9,10]. The competition between self-focusing and diffraction may result in morphological stability along propagation and give rise to optical solitons.

Since the early works about OAM transfer in second harmonic generation, other systems have been studied, such as cold atoms [11,12] and optical parametric oscillators [13,14]. The propagation of structured light in nonlinear media has become an active field of research thanks to numerous techniques for shaping the wavefront of laser beams [15]. Both classical [16–21] and quantum [22,23] optical processes have been studied under structured light driving. Recently, it has been shown that OAM transfer in nonlinear wave mixing occurs under selection rules coupling the angular and radial degrees of freedom [24–31]. Essentially, these rules establish that radial modes are generated from the mixture of counter-rotating beams in up-conversion [24,26] or corotating beams in stimulated down-conversion [29]. The generation of radial

modes in optically thin nonlinear media is essentially governed by the mathematical properties of products between Laguerre—Gaussian (LG) modes [26,32]. However, in four-wave mixing in atomic vapors, in addition to the relative chirality of the interacting beams, the Gouy phase match also plays an essential role due to the optical thickness of the nonlinear medium [30].

In this work, we investigate theoretically the appearance of radial modes when a single input LG beam, with topological charge l_0 and zero radial order, undergoes self-phase modulation inside a Kerr medium. The nonlinear propagation is first described with a perturbative approach, where two distinct regions can be identified according to the Rayleigh distance z_R of the input beam. In the focal zone ($z \ll z_R$), a simple selection rule for radial mode generation is derived once the waist of the mode basis is properly chosen. New LG modes are created with radial numbers ranging between zero and the absolute value of the input topological charge l_0 . In the diffraction zone ($z \gtrsim z_R$), the nonlinear evolution becomes affected by the Gouy phase match and a complex radial structure takes place.

This work is organized as follows. In Sec. II we recall the basic concepts of self-phase modulation in nonlinear Kerr media. In Secs. III and IV we derive a set of coupled nonlinear equations for the mode amplitudes in the Laguerre-Gaussian basis and a perturbative approach to the solution. In Secs. V and VI, we analyze the radial mode generation using first-order perturbation in the focal and diffraction zones, respectively. Section VII is devoted to a numerical analysis, which validates the analytical results presented in the preceding sections. Finally, our conclusions are drawn in Sec. VIII. The transformation between LG modes with different waists is presented in the Appendix.

II. SELF-PHASE MODULATION

Let us consider the propagation of a light beam with frequency ω undergoing self-phase modulation inside a nonlinear Kerr medium with linear index of refraction n . The

*azkhoury@id.uff.br

wave equation for the complex electric field amplitude $\mathcal{E}(\mathbf{r})$ under paraxial propagation is

$$\nabla_{\perp}^2 \mathcal{E}(\mathbf{r}) + 2ik \frac{\partial \mathcal{E}(\mathbf{r})}{\partial z} = -\frac{\omega^2}{\varepsilon_0 c^2} \mathcal{P}^{(3)}(\mathbf{r}), \quad (1)$$

where ∇_{\perp}^2 is the Laplacian operator on the transverse coordinates, $\mathcal{P}^{(3)}(\mathbf{r})$ is the nonlinear polarization of the medium, and $k = n\omega/c$ is the wave number inside the medium. The nonlinear polarization is

$$\mathcal{P}^{(3)}(\mathbf{r}) = 3\varepsilon_0 \chi^{(3)} |\mathcal{E}(\mathbf{r})|^2 \mathcal{E}(\mathbf{r}), \quad (2)$$

where $\chi^{(3)}$ is the third-order nonlinear susceptibility. The nonlinear propagation equation is obtained by plugging Eq. (2) into Eq. (1) as follows:

$$\nabla_{\perp}^2 \mathcal{E}(\mathbf{r}) + 2ik \frac{\partial \mathcal{E}(\mathbf{r})}{\partial z} = -3\chi^{(3)} \frac{\omega^2}{c^2} |\mathcal{E}(\mathbf{r})|^2 \mathcal{E}(\mathbf{r}). \quad (3)$$

In the short propagation range, this nonlinear equation gives rise to the well-known self-phase modulation effect, in which the field intensity alters the effective index of refraction seen by the input beam. This effect couples the amplitude and phase dynamics inside the nonlinear medium, which affects the spatial properties of an incoming Gaussian beam. The transverse variation of the beam intensity produces an effective lens, causing the beam focalization or defocalization, according to the sign of the nonlinear susceptibility. In fact, let us assume a solution to Eq. (3) of the form

$$\mathcal{E}(\mathbf{r}) = \mathcal{A}_0 u(\mathbf{r}) e^{i\theta(\mathbf{r})}, \quad (4)$$

where $u(\mathbf{r})$ is a normalized solution of the paraxial wave equation and $\theta(\mathbf{r})$ is an additional phase term due to the nonlinear response of the medium. Under slow transverse variation ($|\nabla_{\perp} u| |\nabla_{\perp} \theta|, |u \nabla_{\perp}^2 \theta| \ll k u \partial \theta / \partial z$), a simple equation can be easily derived for the phase term

$$\frac{\partial \theta}{\partial z} = \frac{g}{2k} |u(\mathbf{r})|^2, \quad (5)$$

$$g = 3\chi^{(3)} \mathcal{A}_0^2 \frac{\omega^2}{c^2}, \quad (6)$$

with the following trivial solution:

$$\theta(\boldsymbol{\rho}, z) = \frac{g}{2k} \int_0^z |u(\boldsymbol{\rho}, z')|^2 dz', \quad (7)$$

where $\boldsymbol{\rho}$ is the position vector on the plane transverse to the propagation direction z . Therefore, the phase evolution is directly affected by the intensity distribution of the beam, which acts as an effective lens and changes the beam focalization, leading to the well-known effects of self-focusing and -defocusing. Equation (4) is well known and has been used in standard descriptions of self-phase modulation. It provides an accurate description of the self-phase modulation phenomenon for interaction lengths much smaller than the Rayleigh distance. However, the appearance of radial-angular coupling in the nonlinear propagation of an optical vortex cannot be easily seen from this standard approach. Moreover, its validity fails when one considers the nonlinear interaction over distances where diffraction becomes important. We next describe a perturbative approach to the nonlinear interaction and investigate the appearance of radial structures as a result

of self-phase modulation in a Laguerre-Gaussian mode. In addition, the perturbative approach can also be used to describe the nonlinear interaction over distances comparable to the Rayleigh length, where diffraction effects become important.

III. SELF-PHASE MODULATION IN THE LAGUERRE-GAUSS BASIS

We will describe the field dynamics in the LG mode basis, where the orbital angular momentum is well defined. In this basis, the electric field amplitude is decomposed as

$$\mathcal{E}(\mathbf{r}) = \sum_{pl} A_{pl}(z) u_{pl}(\mathbf{r}), \quad (8)$$

where $A_{pl}(z)$ is a slowly varying mode amplitude. The mode functions are given by

$$u_{pl}(\mathbf{r}) = \sqrt{\frac{2}{\pi}} \frac{\mathcal{N}_{pl}}{w(z)} (2\tilde{\rho}_z^2)^{\frac{|l|}{2}} L_p^{|l|}(2\tilde{\rho}_z^2) e^{-(1-i\tilde{z})\tilde{\rho}^2} e^{il\phi} e^{-i\varphi_{pl}}, \quad (9)$$

where we adopt the following definitions:

$$\begin{aligned} w(z) &= w_0 \sqrt{1 + \tilde{z}^2}, \\ \tilde{z} &= z/z_R, \quad \tilde{\rho}_z = \rho/w(z), \\ \varphi_{pl} &= (2p + |l| + 1) \arctan(\tilde{z}), \\ \mathcal{N}_{pl} &= \sqrt{\frac{p!}{(p + |l|)!}}. \end{aligned} \quad (10)$$

Here w_0 is the beam waist, $z_R = \pi w_0^2/\lambda$ is the Rayleigh distance, $p \in \mathbb{N}$ is the radial number, and $l \in \mathbb{Z}$ is the topological charge of the LG mode. When the expansion given by Eq. (8) is substituted in the nonlinear wave equation (3), we obtain a set of coupled nonlinear equations for the mode amplitudes

$$\frac{dA_{pl}}{dz} = i \frac{\omega^2 \chi^{(3)}}{2kc^2} R_{pp_1 p_2 p_3}^{l l_1 l_2 l_3} A_{p_1 l_1} A_{p_2 l_2}^* A_{p_3 l_3}, \quad (11)$$

where we adopt the convention of sum over repeated indices. The intermode coupling is mediated by the four-mode overlap integrals over the transverse plane

$$R_{pp_1 p_2 p_3}^{l l_1 l_2 l_3}(z) = \int u_{pl}^*(\mathbf{r}) u_{p_1 l_1}(\mathbf{r}) u_{p_2 l_2}^*(\mathbf{r}) u_{p_3 l_3}(\mathbf{r}) d^2 \boldsymbol{\rho}, \quad (12)$$

which depend on the longitudinal coordinate z . From these integrals we obtain the selection rules constraining the intermode coupling. When a single LG mode is sent into the nonlinear medium, the overlap integrals determine which modes couple to the input one. In this way, the coupled equations of motion describe the onset of new transverse modes according to the selection rules. Interestingly, a finite number of LG modes arise in the short -range propagation, which can be described by a perturbative solution of the nonlinear wave equation. However, we will show that this finite structure appears in a modified mode basis with reduced waist parameter.

IV. PERTURBATIVE SOLUTION OF THE NONLINEAR PROPAGATION

Let us assume that a single LG mode with waist w_0 , $p = 0$, and $l = l_0$ is sent to the nonlinear medium, so the electric field

at the entrance of the medium is

$$\mathcal{E}(\rho, \phi, 0) = \mathcal{A}_0 u_{0l_0}(\rho, \phi, 0). \quad (13)$$

The strength of the nonlinear response is determined by the nonlinear susceptibility and the amplitude of the input field. In this sense, it will be useful to work with the normalized field $\psi(\mathbf{r}) = w_0 \mathcal{E}(\mathbf{r})/\mathcal{A}_0$ and the normalized coordinates $(\tilde{\rho}, \tilde{z}) = (\rho/w_0, z/z_R)$ to render the nonlinear propagation equation amenable to perturbation

$$\tilde{\nabla}_\perp^2 \psi(\mathbf{r}) + 4i \frac{\partial \psi(\mathbf{r})}{\partial \tilde{z}} = -g |\psi(\mathbf{r})|^2 \psi(\mathbf{r}), \quad (14)$$

where g , defined in Eq. (6), is the perturbation parameter. We can propose a solution in the form of a power series in g ,

$$\psi(\mathbf{r}) = \sum_{n=0}^{\infty} g^n \psi_n(\mathbf{r}), \quad (15)$$

with the initial conditions

$$\begin{aligned} \psi_0(\rho, \phi, 0) &= w_0 u_{0l_0}(\rho, \phi, 0), \\ \psi_n(\rho, \phi, 0) &= 0 \quad (n > 0). \end{aligned} \quad (16)$$

By using the expansion in Eq. (14) and matching the powers of g on both sides, we arrive at a set of inhomogeneous linear equations, the first two being

$$\tilde{\nabla}_\perp^2 \psi_0(\mathbf{r}) + 4i \frac{\partial \psi_0(\mathbf{r})}{\partial \tilde{z}} = 0, \quad (17)$$

$$\tilde{\nabla}_\perp^2 \psi_1(\mathbf{r}) + 4i \frac{\partial \psi_1(\mathbf{r})}{\partial \tilde{z}} = -|\psi_0(\mathbf{r})|^2 \psi_0(\mathbf{r}). \quad (18)$$

The solution of Eq. (17) for the zero-order term is obviously

$$\psi_0(\tilde{\rho}, \phi, \tilde{z}) = w_0 u_{0l_0}(\tilde{\rho}, \phi, \tilde{z}). \quad (19)$$

We can find the first-order term by expanding ψ_1 in the LG basis

$$\psi_1(\mathbf{r}) = w_0 \sum_{pl} a_{pl}(z) u_{pl}(\mathbf{r}). \quad (20)$$

The mode amplitudes satisfy the dynamical equations

$$\frac{da_{pl}}{d\tilde{z}} = \frac{i}{4} R_{p0}^{ll_0}(z), \quad (21)$$

$$R_{p0}^{ll_0}(z) = w_0^2 \int u_{pl}^*(\mathbf{r}) U_{0l_0}(\mathbf{r}) d^2 \rho, \quad (22)$$

where $U_{0l_0}(\mathbf{r}) = |u_{0l_0}(\mathbf{r})|^2 u_{0l_0}(\mathbf{r})$, and the initial conditions are $a_{pl}(0) = 0$. Note that the integrand in Eq. (22) depends on the longitudinal coordinate explicitly through the Gouy phase factors, which do not depend on ρ , and implicitly through the width $w(z)$. Since the integral runs over the entire transverse plane, the implicit dependence is washed out and the Gouy phases can be factorized. Therefore, one can easily deduce that the overlap integral satisfies

$$R_{p0}^{ll_0}(z) = \frac{e^{i\Delta\varphi_{pl}(\tilde{z})}}{1 + \tilde{z}^2} R_{p0}^{ll_0}(0), \quad (23)$$

where $\Delta\varphi_{pl}(\tilde{z}) = \varphi_{pl}(\tilde{z}) - \varphi_{0l_0}(\tilde{z})$. Moreover, due to OAM conservation, $R_{p0}^{ll_0}(0) = 0$ for $l \neq l_0$, so the relevant Gouy

phase difference $\Delta\varphi_{pl_0}(\tilde{z}) = 2p \arctan(\tilde{z})$ depends only on p . Therefore, Eq. (21) can be integrated giving

$$a_{pl}(\tilde{z}) = \frac{i}{4} \Phi_p(\tilde{z}) R_{p0}^{ll_0}(0), \quad (24)$$

where

$$\Phi_p(\tilde{z}) = \int_0^{\tilde{z}} \frac{e^{i\Delta\varphi_{pl_0}(\tilde{z}')}}{1 + \tilde{z}'^2} d\tilde{z}' = \frac{1}{2ip} \left[1 - \left(\frac{1 - i\tilde{z}}{1 + i\tilde{z}} \right)^p \right] \quad (25)$$

is the Gouy phase match function. For $p = 0$, this expression reduces to $\Phi_0(\tilde{z}) = \arctan(\tilde{z})$.

In principle, the perturbative solution involves the contribution of an infinite number of LG modes. However, in the focal zone we can show that the overlap $R_{p0}^{ll_0}(\tilde{z})$ selects a finite number of coupled modes, provided the waist parameter of the mode basis is properly adjusted. As we show next, the proper waist is reduced with respect to the initial beam waist.

V. RADIAL MODE GENERATION IN THE FOCAL ZONE ($\tilde{z} \ll 1$)

Up to first order in \tilde{z} , the solution of Eq. (18) reads

$$\psi_1(\mathbf{r}) = \frac{i\tilde{z}}{4} U_{0l_0}(\rho, 0). \quad (26)$$

In the focal zone, where $z \ll z_R$ and $w(z) \approx w_0$, the mode functions are approximately independent of the longitudinal coordinate z , so that $R_{p0}^{ll_0}(z) \approx R_{p0}^{ll_0}(0)$. In this case, the cubic term in the overlap integral is reduced to

$$U_{0l_0}(\rho, 0) = \left(\sqrt{\frac{2}{\pi}} \frac{\mathcal{N}_{0l_0}}{w_0} \right)^3 \left(\frac{\sqrt{2}\rho}{w_0} \right)^{3|l_0|} e^{-\frac{3\rho^2}{w_0^2}} e^{il_0\phi}. \quad (27)$$

This term can be written as a superposition of pure LG modes with a rescaled waist \bar{w}_0 and Rayleigh distance $\bar{z}_R = \pi \bar{w}_0^2/\lambda$. This is accomplished by inverting the expression of the Laguerre polynomials in terms of monomials to obtain [33]

$$\left(\frac{2\rho^2}{\bar{w}_0^2} \right)^{|l_0|} = |l_0|! \sum_{p=0}^{|l_0|} \binom{|l_0|}{|l_0| - p} (-1)^p L_p^{|l_0|} \left(\frac{2\rho^2}{\bar{w}_0^2} \right), \quad (28)$$

where we made $\bar{w}_0 = w_0/\sqrt{3}$ to match the width of the Gaussian term in Eq. (27). In this way, the cubic term can be written as a superposition of LG modes with the rescaled waist \bar{w}_0 ,

$$U_{0l_0}(\rho, 0) = \frac{1}{w_0^2} \sum_{p=0}^{|l_0|} C_{pl_0} \bar{u}_{pl_0}(\rho, 0), \quad (29)$$

$$C_{pl_0} = \frac{2(-1)^p}{\pi (\sqrt{3})^{3|l_0|+1}} \binom{2|l_0|}{|l_0| - p} \binom{|l_0| + p}{p}^{\frac{1}{2}}, \quad (30)$$

where $\{\bar{u}_{pl}\}$ is the set of LG modes with the rescaled waist. Therefore, in the focal zone, it will be useful to write the first-order solution in terms of these rescaled modes

$$\begin{aligned} \psi_1(\mathbf{r}) &= w_0 \sum_{pl} \bar{a}_{pl}(z) \bar{u}_{pl}(\mathbf{r}), \\ \frac{d\bar{a}_{pl}}{d\tilde{z}} &= \frac{i}{4} \bar{R}_{p0}^{ll_0}(z), \end{aligned} \quad (31)$$

so the overlap integral becomes

$$\bar{R}_{p0}^{l_0}(z) \approx \bar{R}_{p0}^{l_0}(0) = \sum_{q=0}^{|l_0|} C_{ql_0} \int \bar{u}_{pl}^*(\mathbf{r}) \bar{u}_{ql_0}(\mathbf{r}) d^2 \rho. \quad (32)$$

From the orthonormality of the rescaled LG modes, one trivially obtains

$$\bar{a}_{pl} = \frac{i\delta_{l_0}\tilde{z}}{4} \begin{cases} C_{pl_0} & (p \leq |l_0|), \\ 0 & (p > |l_0|). \end{cases} \quad (33)$$

Therefore, the final solution up to first-order perturbation in the short range is

$$\psi(\mathbf{r}) = \psi_0(\mathbf{r}) + \frac{ig\tilde{z}w_0}{4} \sum_{p=0}^{|l_0|} C_{pl_0} \bar{u}_{pl_0}(\mathbf{r}). \quad (34)$$

Therefore, a finite number of radial modes from $p = 0$ to $|l_0|$ arise in the short interaction range. The corresponding mode amplitudes grow linearly until diffraction takes place. Note that the same result could be obtained by expanding the standard solution given in Eq. (4) up to first order in g and taking the limit $z \ll z_R$. However, in the diffraction zone ($\tilde{z} \gtrsim 1$) the Gouy phase match becomes relevant and the self-modulated field undergoes a more involved dynamics. In this case, a simple expansion of the standard solution is no longer applicable, while the perturbative approach, including the Gouy phase matching term, provides the proper description.

VI. NONLINEAR PROPAGATION IN THE DIFFRACTION ZONE ($z \gtrsim z_R$)

In the diffraction zone, the prefactor appearing in Eq. (23) cannot be neglected. Moreover, the transverse overlap at $z = 0$ is

$$\begin{aligned} R_{p0}^{l_0}(0) &= w_0^2 \int u_{pl}^*(\rho, 0) U_{0l_0}(\rho, 0) d^2 \rho \\ &= \sum_{q=0}^{|l_0|} C_{ql_0} \int u_{pl}^*(\rho, 0) \bar{u}_{ql_0}(\rho, 0) d^2 \rho. \end{aligned} \quad (35)$$

Note that the integral appearing in Eq. (35) is simply the coefficient $\Lambda_{qp}^l(3)$ of the mode waist transformation between the bases $\{u_{qm}\}$ and $\{\bar{u}_{qm}\}$ derived in the Appendix. Using this result in Eq. (35), we find

$$R_{p0}^{l_0}(0) = \delta_{l_0} \sum_{q=0}^{|l_0|} \Lambda_{qp}^{l_0}(3) C_{ql_0}. \quad (36)$$

This allows us to find the solution of the dynamical equations (21) for the expansion coefficients in the diffraction zone

$$a_{pl}(\tilde{z}) = \frac{i\delta_{l_0}}{4} \Phi_p(\tilde{z}) \sum_{q=0}^{|l_0|} C_{ql_0} \Lambda_{qp}^{l_0}(3), \quad (37)$$

so the first-order perturbation term becomes

$$\psi(\mathbf{r}) = \psi_0(\mathbf{r}) + \frac{igw_0}{4} \sum_{q=0}^{|l_0|} C_{ql_0} \sum_{p=0}^{\infty} \Phi_p(\tilde{z}) \Lambda_{qp}^{l_0}(3) u_{pl_0}(\mathbf{r}). \quad (38)$$

TABLE I. Characteristic power for some systems. Calculated from Table 4.1.2 of Ref. [34] with $\lambda = 1550$ nm.

Medium	P_{NL} (W)
Fused silica	65
GaAs crystal	2.7×10^{-2}
Gold nanoparticles in glass	7.8×10^{-5}

The short-range solution Eq. (34) is immediately recovered by making $\tilde{z} \ll 1$, so that $\Phi_p(\tilde{z}) \approx \tilde{z} \forall (p, l)$, and noting that

$$\bar{u}_{ql_0}(\mathbf{r}) = \sum_{p=0}^{\infty} \Lambda_{qp}^{l_0}(3) u_{pl_0}(\mathbf{r}). \quad (39)$$

We next compare the analytical results for the radial mode generation with numerical solutions of the nonlinear propagation equation.

VII. NUMERICAL ANALYSIS

Let us now turn to the numerical solution of the nonlinear wave equation (14) and compare the behavior predicted for the short-range propagation with the perturbative solutions described in the preceding sections.

To estimate g in the physically realizable cases, we note that

$$3\chi^{(3)}|\mathcal{E}(\mathbf{r})|^2 = 2n_0n_2I(\mathbf{r}), \quad (40)$$

where $I(\mathbf{r})$ is the intensity of the beam and n_0 (n_2) is the linear (nonlinear) refractive index, such that the total refractive index is given by $n = n_0 + n_2I$ [34]. Integrating both sides of this equation over a transverse plane, we get

$$3\chi^{(3)}\mathcal{A}_0^2 = 2n_0n_2P, \quad (41)$$

where P is the power of the beam. Therefore, we have

$$g = 3\chi^{(3)}\frac{\omega^2}{c^2}\mathcal{A}_0^2 = \frac{8\pi^2n_0n_2}{\lambda^2}P, \quad (42)$$

where λ is the vacuum wavelength. We can define

$$P_{NL} = \frac{\lambda^2}{8\pi^2n_0n_2}, \quad (43)$$

which works as a characteristic power for the nonlinear process. In Table I we show three examples of P_{NL} with different orders of magnitude. It is then safe to assume that g can span values from 10^{-6} to 10.

The numerical integration was done using a type-2A step-splitting algorithm [35,36], which is implemented by the package STRUCTURED LIGHT.JL [37]. The code used to produce the results of this paper can be accessed at [38].

First, we get a numerical solution of (14), then we compute the quantity

$$\delta\psi = \frac{\psi - \psi_0}{g} = \psi_1 + \mathcal{O}(g), \quad (44)$$

and the projections

$$c_{pl_0} = \frac{1}{w_0} \int \bar{u}_{pl_0}^*(\tilde{\mathbf{r}}) \delta\psi(\tilde{\mathbf{r}}) d^2 \rho. \quad (45)$$

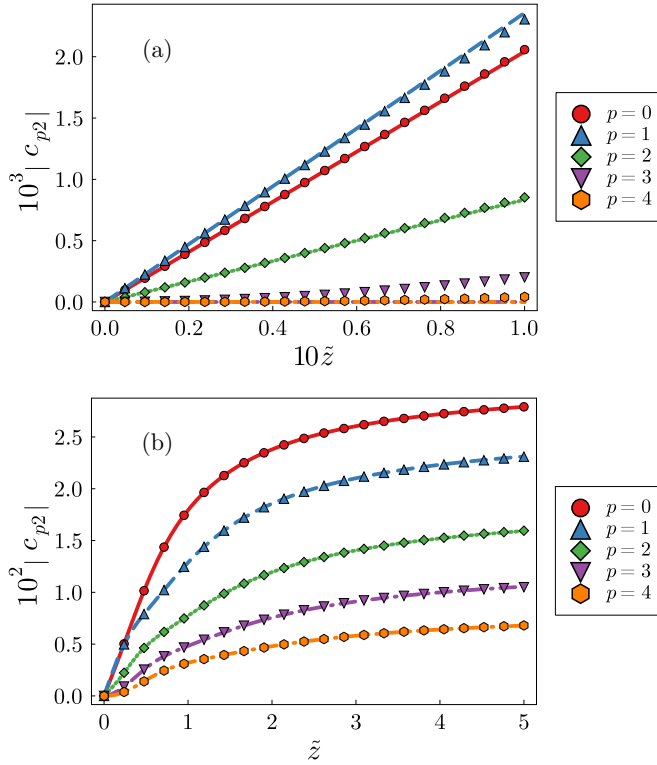


FIG. 1. Overlap coefficients c_{p2} for $g = 0.01$ and $l_0 = 2$. In (a), we illustrate the short-range propagation, where the solid lines represent the approximation given in Eq. (47). The appearance of radial modes with $0 \leq p \leq 2$ is clear. In (b) we show the diffraction zone, where more radial modes are generated. In both cases lines represent the approximation given by Eq. (46) and markers represent the results obtained from numerical integration of the nonlinear wave equation for $p = 0$ (red solid line and circles), $p = 1$ (blue dashed line and up triangles), $p = 2$ (green dotted line and diamonds), $p = 3$ (purple dash-dotted line and down triangles), and $p = 4$ (orange dashed-double-dotted line and hexagons).

According to Eq. (38), up to first-order perturbation, we should have

$$c_{pl_0} \approx \frac{i}{4} \sum_{q=0}^{|l_0|} C_{ql_0} \sum_{r=0}^{\infty} \Phi_r(\tilde{z}) \Lambda_{pr}^{l_0}(3) \Lambda_{qr}^{l_0}(3), \quad (46)$$

where the summation over r will actually be truncated at some sufficiently large value r_{\max} for numerical comparison. Note that, for $\tilde{z} \ll 1$, we have $\Phi_r(\tilde{z}) \approx \tilde{z}$. In addition, as a basis transformation, $\Lambda_{pr}^{l_0}(\eta)$ must be an orthogonal matrix, so that $\sum_r \Lambda_{pr}^{l_0}(\eta) \Lambda_{qr}^{l_0}(\eta) = \delta_{pq}$, which leads to

$$c_{pl_0} \approx \frac{i}{4} \tilde{z} C_{pl_0}. \quad (47)$$

Our numerical calculations will cover the two regimes corresponding to the focal ($z \ll z_R$) and diffraction zones ($z \gtrsim z_R$). The values assumed for the nonlinear coupling g will fall in the physical range given by Table I. In Fig. 1, we plot the results for $g = 0.01$ and $l_0 = 2$ in the focal and diffraction zones. This corresponds to a 1550 nm wavelength laser with 650 mW power propagating in fused silica, for example. For the diffraction zone solution, the summation

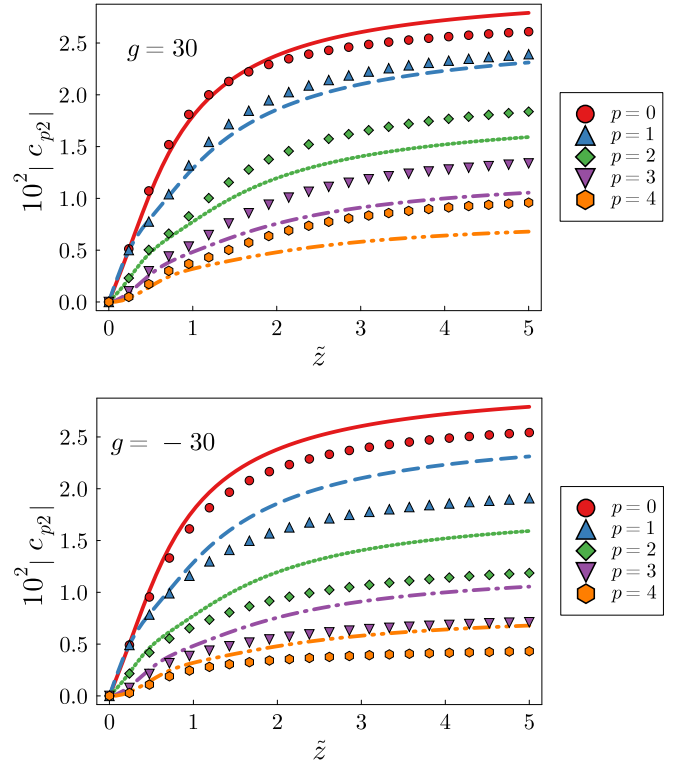


FIG. 2. Overlap coefficients c_{p2} for $g = \pm 30$. The solid lines represent the approximation given by Eq. (46). In both cases lines represent the approximation given by Eq. (46) and markers represent the results obtained from numerical integration of the nonlinear wave equation for $p = 0$ (red solid line and circles), $p = 1$ (blue dashed line and up triangles), $p = 2$ (green dotted line and diamonds), $p = 3$ (purple dash-dotted line and down triangles), and $p = 4$ (orange dashed-double-dotted line and hexagons).

over r was truncated at $r_{\max} = 10^3$. One can easily see the development of a finite radial spectrum in the focal zone, with $0 \leq p \leq 2$, while other radial modes appear in the diffraction zone. The results obtained from the perturbative expressions are in excellent agreement with those given by numerical integration of the nonlinear wave equation. Interestingly, the perturbative approach works well for $g \sim 1$, with significant deviations appearing for $g \gtrsim 10$, as shown in Fig. 2. Note that $\delta\psi$ defined in Eq. (44) is insensitive to the sign of g up to first-order perturbation, so that discrepancies only appear for $g \gtrsim 10$, where second-order corrections become important. These results may be easily investigated with reasonable powers in fused silica, for example. Moreover, in atomic vapors both the magnitude and sign of g can be varied [39].

The appearance of rings with Gaussian beams in self-phase modulation was thoroughly investigated in Ref. [40]. It was later used to measure the nonlinear response of an atomic vapor [39]. However, these studies did not consider the effects caused by the orbital angular momentum. We next show numerical simulations of the radial mode generation under the physical conditions used in Ref. [39]. In Fig. 3 we show the numerical results for the expansion coefficients of $\delta\psi$ for $l_0 = 0$ and 2 under the experimental conditions. The values of the coupling parameter g were set to correspond to the same peak intensity for all OAM values. It is straightforward to

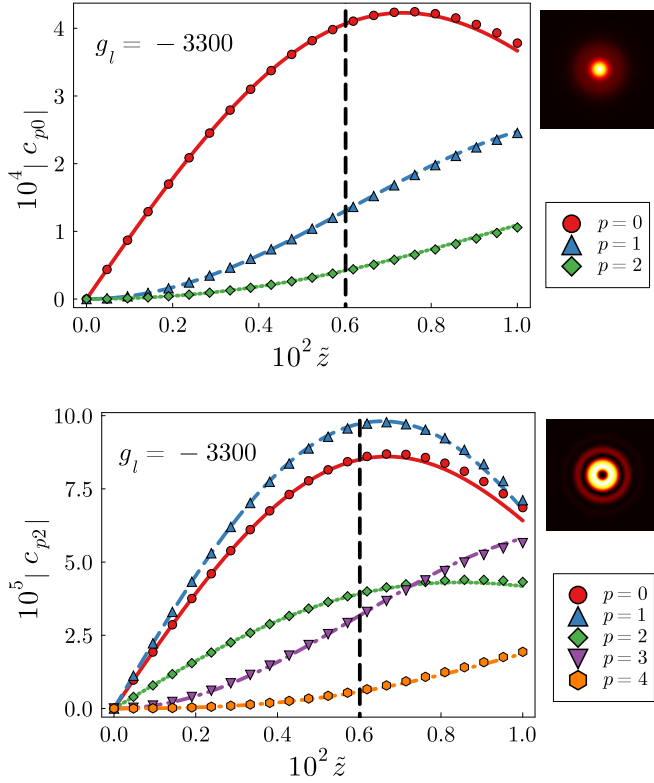


FIG. 3. Overlap coefficients for $g_l = -3300$, corresponding to the experimental conditions of Ref. [39]. Top: $l_0 = 0$ (c_{p0}). Bottom: $l_0 = 2$ (c_{p2}). The vertical dashed line indicates the interaction length in the experiment. The insets show the simulated far field images. In both cases lines represent the approximation given by Eqs. (4) and (7) and markers represent the results obtained from numerical integration of the nonlinear wave equation for $p = 0$ (red solid line and circles), $p = 1$ (blue dashed line and up triangles), $p = 2$ (green dotted line and diamonds), $p = 3$ (purple dash-dotted line and down triangles), and $p = 4$ (orange dashed-double-dotted line and hexagons).

demonstrate that for a fixed beam power P , the peak intensity over the transverse plane is given by

$$I_{\max}^l = I_0 \frac{|l|^{|l|} e^{-|l|}}{|l|!} \approx \frac{I_0}{\sqrt{2\pi|l|}}, \quad (48)$$

where the approximation follows from Stirling's formula and $I_0 = 2P/(\pi w_0^2)$ is the peak intensity of a Gaussian beam. Therefore, it will be useful to define

$$g_l = g \frac{|l|^{|l|} e^{-|l|}}{|l|!} \approx \frac{g}{\sqrt{2\pi|l|}}, \quad (49)$$

where the final approximation holds for $|l| > 0$. A meaningful comparison between the nonlinear effects on different OAM values must involve similar values of g_l rather than g . For $l = 0$ the radial mode components appear only in the non-perturbative region and add up to the input mode, forming the far-field ring structure. For $l = 2$ the radial modes appear already in the perturbative region, causing a more pronounced ring structure in the far field. One can easily see that only the radial modes with $0 \leq p \leq |l_0|$ have nonzero derivative at

$z = 0$, as expected from the perturbative solution in the focal zone.

VIII. CONCLUSION

In this work we analyze the generation of a radial mode structure along propagation of an optical vortex inside a nonlinear Kerr medium. Our analysis is based on a perturbative approach, useful for sufficiently small nonlinear interaction. In this regime, the radial mode structure appears in the short range according to a simple selection rule, once the waist of the mode basis is properly set. Radial numbers ranging between zero and the absolute value of the input topological charge are generated. In the diffraction zone, the radial mode intensity distribution is significantly affected by the Gouy phase match, an effect also observed in intracavity parametric down-conversion [41] and four-wave mixing [30]. Our analytical results obtained with the perturbative solution are legitimated by the numerical integration of the nonlinear wave equation. Our results can be useful for a wide variety of physical systems displaying self-phase modulation, such as optical propagation in atomic vapors and optical fibers. These methods can also be useful to describe the evolution of vortex structures in Bose-Einstein condensates. A promising lead to the present project is the investigation of quantum correlations associated with the radial mode generation in the self-modulation process. The methods presented here will serve as the basis of a quantum description, where the radial mode amplitudes are quantized.

ACKNOWLEDGMENTS

Funding was provided by Conselho Nacional de Desenvolvimento Científico e Tecnológico (CNPq), Coordenação de Aperfeiçoamento de Pessoal de Nível Superior (CAPES), Fundação Carlos Chagas Filho de Amparo à Pesquisa do Estado do Rio de Janeiro (FAPERJ), Instituto Nacional de Ciência e Tecnologia de Informação Quântica (INCT-IQ 465469/2014-0) and Fundação de Amparo à Pesquisa do Estado de São Paulo (FAPESP, Grant No. 2021/06823-5). A.Z.K. acknowledges financial support from Centre National de la Recherche Scientifique (CNRS) during his two-month stay at Laboratoire Kastler Brossel (LKB).

APPENDIX: CONVERSION BETWEEN MODE FAMILIES WITH DIFFERENT WAISTS

In this Appendix we derive the transformation connecting two LG mode families with different waist parameters. It will help the identification of the optimal waist parameter for minimizing the number of radial modes in the short range. Let us consider two LG mode families $\{u_{pl}(\mathbf{r})\}$ and $\{\bar{u}_{pl}(\mathbf{r})\}$, with different waist parameters and Rayleigh distances. Suppose their Rayleigh distances are related by $z_R = \eta \bar{z}_R$, which implies $w_0^2 = \eta \bar{w}_0^2$. We want to determine the coefficients $\{\Lambda_{qp}^{ml}\}$ such that

$$\bar{u}_{qm}(\mathbf{r}) = \sum_{pl} \Lambda_{qp}^{ml}(\eta) u_{pl}(\mathbf{r}). \quad (A1)$$

The transformation coefficients are obtained by projecting Eq. (A1) onto the $\{u_{pl}(\mathbf{r})\}$ basis. Since the coefficients do not depend on the longitudinal coordinate z , we can calculate the transformation coefficients at $z = 0$. Therefore,

$$\begin{aligned}\Lambda_{qp}^{ml}(\eta) &= \int \bar{u}_{qm}(\boldsymbol{\rho}, 0) u_{pl}^*(\boldsymbol{\rho}, 0) d^2 \boldsymbol{\rho} \\ &= \frac{2}{\pi} \mathcal{N}_{qm} \mathcal{N}_{pl} (\sqrt{\eta})^{|m|+1} \int_0^{2\pi} e^{i(m-l)\phi} d\phi \\ &\quad \times \int_0^\infty (2\tilde{\rho}^2)^{\frac{|m|+|l|}{2}} L_q^{||} (2\eta\tilde{\rho}^2) L_p^{||} (2\tilde{\rho}^2) e^{-(\eta+1)\tilde{\rho}^2} \tilde{\rho} d\tilde{\rho},\end{aligned}\quad (\text{A2})$$

where $\tilde{\rho} = \rho^2/w_0^2$. Of course, the topological charges are not altered by a change in the waist, so the angular integral imposes $l = m$, leading to

$$\Lambda_{qp}^l(\eta) = \mathcal{N}_{ql} \mathcal{N}_{pl} \lambda_{qp}^l(\eta), \quad (\text{A3})$$

where we drop one superfluous upper index in Λ_{qp}^l and define

$$\lambda_{qp}^l(\eta) = (\sqrt{\eta})^{|l|+1} \int_0^\infty x^{|l|} L_q^{||}(\eta x) L_p^{||}(x) e^{-\alpha x} dx, \quad (\text{A4})$$

with $x = 2\tilde{r}^2$ and $\alpha = (\eta + 1)/2$. The integral $\lambda_{qp}^l(\eta)$ can be obtained by using the generating function for the generalized

Laguerre polynomials

$$L_p^{||}(x) = \frac{1}{p!} \frac{\partial^p}{\partial t^p} \left[\frac{e^{-xt/(1-t)}}{(1-t)^{|l|+1}} \right] \Bigg|_{t=0}, \quad (\text{A5})$$

which leads to

$$\begin{aligned}\lambda_{qp}^l(\eta) &= \frac{(\sqrt{\eta})^{|l|+1}}{q!p!} \frac{\partial^q}{\partial t'^q} \frac{\partial^p F}{\partial t^p} \Bigg|_{t,t'=0}, \\ F(t, t') &= \frac{1}{[(1-t')(1-t)]^{|l|+1}} \int_0^\infty x^{|l|} e^{-bx} dx \\ &= \frac{|l|!}{[b(1-t')(1-t)]^{|l|+1}}, \\ b &= \frac{\eta t'}{1-t'} + \frac{t}{1-t} + \alpha.\end{aligned}\quad (\text{A6})$$

After a straightforward algebra, we arrive at

$$\begin{aligned}\Lambda_{qp}^l(\eta) &= (-1)^p \mathcal{N}_{ql} \mathcal{N}_{pl} \left(\frac{2\sqrt{\eta}}{1+\eta} \right)^{|l|+1} \\ &\quad \times \sum_{n=0}^p (-1)^n \frac{(q+p+|l|-n)!}{n!(p-n)!(q-n)!} \left(\frac{1-\eta}{1+\eta} \right)^{q+p-2n}.\end{aligned}\quad (\text{A7})$$

In the main text we use this mode conversion formula with $\eta = 3$ to determine the overlap integral.

-
- [1] K. Dholakia, N. B. Simpson, M. J. Padgett, and L. Allen, Second-harmonic generation and the orbital angular momentum of light, *Phys. Rev. A* **54**, R3742 (1996).
- [2] J. Courtial, K. Dholakia, L. Allen, and M. J. Padgett, Second-harmonic generation and the conservation of orbital angular momentum with high-order laguerre-gaussian modes, *Phys. Rev. A* **56**, 4193 (1997).
- [3] A. Mair, A. Vaziri, G. Weihs, and A. Zeilinger, Entanglement of the orbital angular momentum states of photons, *Nature (London)* **412**, 313 (2001).
- [4] D. P. Caetano, M. P. Almeida, P. H. Souto Ribeiro, J. A. O. Huguenin, B. Coutinho dos Santos, and A. Z. Khoury, Conservation of orbital angular momentum in stimulated down-conversion, *Phys. Rev. A* **66**, 041801(R) (2002).
- [5] A. E. Willner, H. Huang, Y. Yan, Y. Ren, N. Ahmed, G. Xie, C. Bao, L. Li, Y. Cao, Z. Zhao, J. Wang, M. P. J. Lavery, M. Tur, S. Ramachandran, A. F. Molisch, N. Ashrafi, and S. Ashrafi, Optical communications using orbital angular momentum beams, *Adv. Opt. Photon.* **7**, 66 (2015).
- [6] L. Gong, Q. Zhao, H. Zhang, X.-Y. Hu, K. Huang, J.-M. Yang, and Y.-M. Li, Optical orbital-angular-momentum-multiplexed data transmission under high scattering, *Light Sci. Appl.* **8**, 27 (2019).
- [7] P. Gregg, P. Kristensen, A. Rubano, S. Golowich, L. Marrucci, and S. Ramachandran, Enhanced spin orbit interaction of light in highly confining optical fibers for mode division multiplexing, *Nat. Commun.* **10**, 4707 (2019).
- [8] N. Bloembergen, *Nonlinear Optics* (Pearson Addison-Wesley, New York, 1977).
- [9] F. Dalfovo, S. Giorgini, L. P. Pitaevskii, and S. Stringari, Theory of bose-einstein condensation in trapped gases, *Rev. Mod. Phys.* **71**, 463 (1999).
- [10] J. T. Mendonça, R. Bingham, and P. Shukla, A kinetic approach to bose-einstein condensates: Self-phase modulation and bogoliubov oscillations, *J. Exp. Theor. Phys.* **101**, 942 (2005).
- [11] J. W. R. Tabosa and D. V. Petrov, Optical Pumping of Orbital Angular Momentum of Light in Cold Cesium Atoms, *Phys. Rev. Lett.* **83**, 4967 (1999).
- [12] S. Barreiro and J. W. R. Tabosa, Generation of Light Carrying Orbital Angular Momentum via Induced Coherence Grating in Cold Atoms, *Phys. Rev. Lett.* **90**, 133001 (2003).
- [13] M. Martinelli, J. A. O. Huguenin, P. Nussenzveig, and A. Z. Khoury, Orbital angular momentum exchange in an optical parametric oscillator, *Phys. Rev. A* **70**, 013812 (2004).
- [14] R. B. Rodrigues, J. Gonzales, B. P. da Silva, J. A. O. Huguenin, M. Martinelli, R. M. de Araújo, C. E. R. Souza, and A. Z. Khoury, Orbital angular momentum symmetry in a driven optical parametric oscillator, *Opt. Lett.* **43**, 2486 (2018).
- [15] N. Matsumoto, T. Ando, T. Inoue, Y. Ohtake, N. Fukuchi, and T. Hara, Generation of high-quality higher-order laguerre-gaussian beams using liquid-crystal-on-silicon spatial light modulators, *J. Opt. Soc. Am. A* **25**, 1642 (2008).
- [16] W. T. Buono, L. F. C. Moraes, J. A. O. Huguenin, C. E. R. Souza, and A. Z. Khoury, Arbitrary orbital angular momentum

- addition in second harmonic generation, *New J. Phys.* **16**, 093041 (2014).
- [17] R. Généaux, A. Camper, T. Auguste, O. Gobert, J. Caillat, R. Taïeb, and T. Ruchon, Synthesis and characterization of attosecond light vortices in the extreme ultraviolet, *Nat. Commun.* **7**, 12583 (2016).
- [18] A. S. Rao, Characterization of off-axis phase singular optical vortex and its nonlinear wave-mixing to generate control broad OAM spectra, *Phys. Scr.* **95**, 055508 (2020).
- [19] M. Fanciulli, D. Bresteau, M. Vimal, M. Luttmann, M. Sacchi, and T. Ruchon, Electromagnetic theory of helicoidal dichroism in reflection from magnetic structures, *Phys. Rev. A* **103**, 013501 (2021).
- [20] H.-J. Wu, B.-S. Yu, Z.-H. Zhu, W. Gao, D.-S. Ding, Z.-Y. Zhou, X.-P. Hu, C. Rosales-Guzmán, Y. Shen, and B.-S. Shi, Conformal frequency conversion for arbitrary vectorial structured light, *Optica* **9**, 187 (2022).
- [21] B. P. da Silva, W. T. Buono, L. J. Pereira, D. S. Tasca, K. Dechoum, and A. Z. Khoury, Spin to orbital angular momentum transfer in frequency up-conversion, *Nanophotonics* **11**, 771 (2022).
- [22] C. E. Vollmer, C. Baune, A. Sambrowski, T. Eberle, V. Händchen, J. Fiurášek, and R. Schnabel, Quantum Up-Conversion of Squeezed Vacuum States from 1550 to 532 nm, *Phys. Rev. Lett.* **112**, 073602 (2014).
- [23] H. Kerdoncuff, J. B. Christensen, and M. Lassen, Quantum frequency conversion of vacuum squeezed light to bright tunable blue squeezed light and higher-order spatial modes, *Opt. Express* **29**, 29828 (2021).
- [24] L. J. Pereira, W. T. Buono, D. S. Tasca, K. Dechoum, and A. Z. Khoury, Orbital-angular-momentum mixing in type-II second-harmonic generation, *Phys. Rev. A* **96**, 053856 (2017).
- [25] W. T. Buono, J. Santiago, L. J. Pereira, D. S. Tasca, K. Dechoum, and A. Z. Khoury, Polarization-controlled orbital angular momentum switching in nonlinear wave mixing, *Opt. Lett.* **43**, 1439 (2018).
- [26] W. T. Buono, A. Santos, M. R. Maia, L. J. Pereira, D. S. Tasca, K. Dechoum, T. Ruchon, and A. Z. Khoury, Chiral relations and radial-angular coupling in nonlinear interactions of optical vortices, *Phys. Rev. A* **101**, 043821 (2020).
- [27] H.-J. Wu, H.-R. Yang, C. Rosales-Guzmán, W. Gao, B.-S. Shi, and Z.-H. Zhu, Vectorial nonlinear optics: Type-II second-harmonic generation driven by spin-orbit-coupled fields, *Phys. Rev. A* **100**, 053840 (2019).
- [28] H.-J. Wu, L.-W. Mao, Y.-J. Yang, C. Rosales-Guzmán, W. Gao, B.-S. Shi, and Z.-H. Zhu, Radial modal transitions of laguerre-gauss modes during parametric up-conversion: Towards the full-field selection rule of spatial modes, *Phys. Rev. A* **101**, 063805 (2020).
- [29] A. G. de Oliveira, G. Santos, N. R. da Silva, L. J. Pereira, G. B. Alves, A. Z. Khoury, and P. H. Souto Ribeiro, Beyond Conservation of Orbital Angular Momentum in Stimulated Parametric Down-Conversion, *Phys. Rev. Appl.* **16**, 044019 (2021).
- [30] R. F. Offer, A. Daffurn, E. Riis, P. F. Griffin, A. S. Arnold, and S. Franke-Arnold, Gouy phase-matched angular and radial mode conversion in four-wave mixing, *Phys. Rev. A* **103**, L021502 (2021).
- [31] M. R. L. da Motta, A. A. C. de Almeida, and S. S. Vianna, Spatial distribution of two symmetric four-wave-mixing signals induced by gaussian beams, *Phys. Rev. A* **106**, 053502 (2022).
- [32] V. V. Kotlyar, E. G. Abramochkin, A. A. Kovalev, and A. A. Savelyeva, Product of two laguerre-gaussian beams, *Photonics* **9**, 496 (2022).
- [33] G. B. Arfken, H.-J. Weber, and F. E. Harris, *Mathematical Methods for Physicists: A Comprehensive Guide* (Elsevier, Amsterdam, 2013).
- [34] R. W. Boyd, *Nonlinear Optics* (Academic, New York, 2020).
- [35] W. Bao, D. Jaksch, and P. A. Markowich, Numerical solution of the gross-pitaevskii equation for bose-einstein condensation, *J. Comput. Phys.* **187**, 318 (2003).
- [36] S. A. Chin, Structure of numerical algorithms and advanced mechanics, *Am. J. Phys.* **88**, 883 (2020).
- [37] M. Gil de Oliveira, StructuredLight.jl, <https://github.com/marcgil/StructuredLight.jl/tree/master>.
- [38] M. Gil de Oliveira, RadialAngularCouplingKerr, <https://github.com/marcgil/RadialAngularCouplingKerr>.
- [39] N. Šantić, A. Fusaro, S. Salem, J. Garnier, A. Picozzi, and R. Kaiser, Nonequilibrium Precondensation of Classical Waves in Two Dimensions Propagating through Atomic Vapors, *Phys. Rev. Lett.* **120**, 055301 (2018).
- [40] E. V. G. Ramirez, M. L. A. Carrasco, M. M. M. Otero, S. C. Cerda, and M. D. I. Castillo, Far field intensity distributions due to spatial self phase modulation of a Gaussian beam by a thin nonlocal nonlinear media, *Opt. Express* **18**, 22067 (2010).
- [41] G. B. Alves, R. F. Barros, D. S. Tasca, C. E. R. Souza, and A. Z. Khoury, Conditions for optical parametric oscillation with a structured light pump, *Phys. Rev. A* **98**, 063825 (2018).